LIFETIMES OF THE $2s^22p\ ^2P^o$- $2s2p^2\ ^4P$ INTERCOMBINATION TRANSITIONS OF C^+

S. J. Smith, A. Chutjian and J. B. Greenwood*

Jet Propulsion Laboratory, California Institute of Technology

Pasadena, CA 91109 USA

ABSTRACT

Radiative Einstein A-values have been measured for fine structure transitions in the intercombination $2s2p^2\ ^4P \rightarrow 2s^22p\ ^2P^o$ decay in C^+. Use was made of a new Kingdon ion trap installed on a beam line for highly-charged ions. The measured radiative rates A_J are 130.0 ± 5.5 s^{-1} for the $^4P_{1/2}$ sublevel, 9.0 ± 1.0 s^{-1} for the $^4P_{3/2}$ sublevel, and 50.0 ± 2.5 s^{-1} for the $^4P_{5/2}$ sublevel. Comparisons with other measurements and results of theories are given.

PACS numbers: 32.70Cs, 32.80Pj, 95.30 Dr, 95.30 Jx

*Present address: Dept. Pure and Applied Physics

Queen's University Belfast, BT7 1NN United Kingdom

I. INTRODUCTION

Emission lines of boron-like carbon are prevalent in astrophysical objects. They are observed regularly in planetary nebulae [1], galactic low-ionization nuclear emission-line regions (LINERS)[2], and in N-type carbon stars [3]. In laboratory fusion plasmas, much of the radiated power near the tokamak diverter comes from carbon emission lines, and the power in the carbon ions becomes a good measure of the total radiated power from the plasma [4]. In all cases, the level populations are determined by competition between collisional excitation, requiring electron excitation cross sections; and radiative decay, requiring spontaneous Einstein A-values and lifetimes.

Reported herein are measurements of radiative decay lifetimes for the intercombination $2s2p^2\ {}^4P \rightarrow 2s^22p\ {}^2P^o$ decay in C^+. This work complements measurements of the absolute excitation cross sections in this transition reported earlier [5]. The lifetime measurements were made using a Kingdon ion trap on a dedicated beam line with an electron-cyclotron resonance (ECR) ion source [6]. Two previous measurements of these lifetimes has used a radiofrequency ion trap with the C^+ ions generated by *in situ* electron-impact ionization of CO [7]; and by use of an ion storage ring using optical detection and light-collecting optics [8]. Results of several theoretical calculations are also available [9-12]. The present work differs from that of Ref. [7] in that different traps were used, and present measurements did not require *in situ* ionization of a feed gas, and hence were carried out at trap background pressures of more than an order of magnitude lower.

II. EXPERIMENTAL METHODS

A. Ion Beam Line and Kingdon Ion Trap

This paper present first results of lifetime measurements on a new Kingdon ion trap installed on a highly-charge ion (HCl) beam line using the *Caprice* ECR ion source [6]. The aim of this work is to provide lifetimes in the range 0.001 to 1.0 s, at the 5-8% level of accuracy in those HCIs which are important emitters in astrophysical and tokamak plasmas. Dipole allowed, so-called E1 transitions, levels decay typically with lifetimes of the order 10 ns or less. Levels with lifetimes in the 0.001 - 1 s range decay *via* intercombination (spin-forbidden) E1, electric quadrupole E2, magnetic dipole M1, and *via* two-photon decays. The C^+ intercombination E1 decay $^4P \rightarrow {}^2P^o$ consists of five lines corresponding to transitions between fine-structure levels in the ground and excited states. A level diagram for the transitions is given in Fig. 1. The emission wavelengths are 2326.09 Å, 2327.62 Å, 2324.19 Å, 2328.82 Å, and 2325.38 Å [13].

The mean life $\tau_J = A_J^{-1}$ of an upper level J is related to the Einstein emission rates A_{iJ} to n lower levels i through the standard expression,

$$\tau_J^{-1} = A_J = \sum_{i=1}^{n} A_{iJ} \, . \tag{1}$$

For an emission wavelength in Å, and for level statistical weights g_i and g_J, the absorption oscillator strength f_{iJ} and the A-value are related through the expression,

$$A_{Ji} = \frac{6.670\times10^{15}}{\lambda^2}\frac{g_i}{g_J}f_{iJ}\,. \tag{2}$$

A schematic of the complete HCI beam line may be found in Ref. [6]. Basically, it consists of an ECR ion source, a mass/charge selection magnet, followed by a three-way electrostatic beam switcher which can route the HCI beam into one of three experimental systems. The first is a merged-beams system dedicated to studying excitation using electron energy loss [14], the second a gas cell and retarding-potential charge-exchange system [15], and the third a Kingdon ion trap for studying metastable lifetimes.

A schematic diagram of this last system alone is given in Fig. 2. The C^+ ions are generated in the *Caprice* ECR using CS_2 as the feed gas, with no additional support gas (usually O_2) used. Approximately 60 W of 14.0 GHz microwave power was used. The extracted ions are mass/charge selected and, after the switcher SW, focused by means of lenses L1 (three element) and L2 (two element) into the center of the Kingdon trap. The extraction voltage at the ECR was 5.2 keV, and ions with lifetimes longer than about 50 μs survive the transit to the trap.

Metastable C^+ ions are routinely produced within the ECR. In our experience, the metastable content of the beam can be varied by adjusting the CS_2 gas pressure, 14 GHz microwave power and the strength of the confining solenoidal magnetic field [5]. By thus "tuning", coupled with use of the beam attenuation method [5], it is found that this content could be adjusted from 0-25%. The higher values are maintained for lifetime measurements herein, and the lower values for excitation measurements.

Details of the electrostatics [16,17] and operational use [18,19] of the Kingdon trap have been presented elsewhere, and only a summary is given here. The trap consists of an aluminum cylinder, 15 cm long and 10 cm diameter. It is perforated at its midplane by four equally-spaced 2.6 cm dia holes to allow entry of the incident ion beam, then exit into a Faraday cup when the trap is "off"; exit of the decay photons into a multiplier phototube; and pulsed ejection of the trapped ions into a microchannel plate. The open ends of the cylinder are covered by two electrically-insulated circular plates. These are always held at a potential of +200 V relative to the cylinder. The trap has a central electrode which is a 0.1 mm dia tungsten wire used to establish the trapping potential with respect to the cylinder. During operation the cylinder and wire are held at about +5.1 kV potential so that the singly-charged ions have energy (5.2 - 5.1) = 0.1 keV in electrode L2 and the trap (trap "off" condition). Ions are thus strongly decelerated and focused into the trap by L2 with a tunable angular width (providing initial angular momentum into the trap) to give maximum trapping. The trap is turned "on" by rapidly pulsing the central wire from its 5.1 kV potential to 2.5 kV with a fall time of less than 100 ns. A thyratron pulser is used, and approximately 6×10^6 ions/particle microampere are trapped. At the same time a voltage is applied to a deflector in a three-element further upstream (before the selection magnet) to prevent additional ions from reaching the trap during the photon-decay period. This voltage risetime is slower, but faster than the equilibration time of the ions in the trap, which is about 2 ms.

The confined ions orbit the central wire. They emit radiation corresponding the metastable decay rate, and they undergo charge-exchanging collisions within the trap through collisions with the background gas. After a time determined by the lifetime component being measured, the central wire is slowly raised (risetime of about 1 ms) and the remaining ions in the trap are accelerated towards the microchannel plate (Fig. 2). This sequence is repeated at a rate of about 1-5 Hz. Because of charge-exchanging collisions the number of ions in the trap will depend on storage time. The population was determined to vary exponentially with storage time, and had a loss time constant of τ_{trap} = 630 ms for an operating pressure of 1.2×10^{-7} Pa (base pressure of 8×10^{-8} Pa). The range of lifetimes that can be measured in the trap is determined at the short end by the trap settling time ($\approx$ 1-2 ms) and at the long end by the trap collisional decay time ($\approx$ 1 s). The five separate optical wavelengths are not resolved, but are detected using 5 cm-dia collimation and focusing lenses, and a custom narrow-band (20 nm, FWHM) interference filter peaked at 232 nm. The lenses are plano-convex, of UV-grade quartz, and are placed within the vacuum chamber, exterior to the trap cylinder. The photon detector and filter were exterior to the fused-quartz window of the vacuum chamber. A UV-grade photomultiplier tube was operated in the pulse-counting mode. The output pulses were amplified, filtered, and counted by a PC-based 256-channel scaler. This MCS was be operated at various scanning times, with a temporal resolution varying from 0.1 to 10 ms/channel, depending on the lifetime component being studied.

B. Data Acquisition and Statistics

The detected photon pulses *vs.* ion storage time were fitted by four exponential terms corresponding to the decay of the three metastable $^4P_{1/2}$, $^4P_{3/2}$, and $^4P_{5/2}$ levels, and the exponential decay of the trap population. A constant background corresponding to the phototube dark current was also included. In treating the data in the present case the assumption is made that, because of the low pressures in the trap, ion-gas quenching is negligible. In the analysis of Fang *et al.* [7] this corresponds to their condition $|S_{ij}| << 1$ where i and j are sublevels in the ^4P state. That assumption was made in Ref. [7] at a background pressure of order 10^{-6} Pa, and is made here with a background of less than 10^{-7} Pa. The detected photon signal I as a function of time t after trapping can then be written as the sum of three exponential decays with initial populations I_1, I_2, and I_3, and Einstein rates $A_{1/2}$, $A_{3/2}$ and $A_{5/2}$ given by, in the simplest case,

$$I = I_1 e^{-A_{1/2}t} + I_2 e^{-A_{3/2}t} + I_3 e^{-A_{5/2}t} . \tag{3}$$

In practice, many runs over several days were carried out of the exponential decay in Eq. (3). One complete data run consisted of 500 fill/dump cycles of the trap, with the decay in each fill cycle recorded in 256 channels. This required about 500 s. Some added time was also taken to retune the ECR and beam line for C^+ metastable-state optimization. A full measurement on any day consisted of 30-50 such cycles, and all data were recorded in a total of 410 measurements spread out over several weeks.

Also, in decay-curve measurements of this type one usually stacks data from all runs on all days into one cumulative exponential decay curve. In the present work data from different runs were kept separate, and the transition rates and uncertainties for each level was evaluated for each run. In practice, it was found that the metastable population in the C^+ beam (and hence the signal to noise) varied from day to day, even when attempting to keep identical tuning conditions of the ECR.

Also, because there is a good separation in the decay rates (factors of three to five between sublevels) data were often recorded by varying the time resolution of the MCS, and recording the short-lifetimes data on some runs, and the longer-lifetime components on others. This again made it difficult to combine all data for a grand total stacked set, but rather each days' run was analyzed separately, and statistical errors computed separately. A full measurement consisted of the data set $d_i(t)$ for $i = \{1,256\}$. Each measurement was then fitted in terms of a model lineshape consisting of a five-exponential function $\mathscr{F}$(t) and a constant background given by,

$$\mathscr{F}(t) = Be^{-r_B t_B} + S_o + \sum_{j=1}^{4} S_j e^{-r_j t}\,, \tag{4}$$

where the S_j and r_j ($j = 1,2,3$) are amplitudes and rates of each upper fine-structure level. In addition a decay term $S_4\, exp(-r_4 t)$ described the brief instability of the trap for the first two milliseconds while ion orbits stabilized. The term $B\, exp(-r_B t)$ is a background decay term corresponding to generation of 232 nm photons from collisions of the trapped C^+ ions with the trap wall, central wire, or quartz lens (collisions with the low density of background gas gave negligible contribution). Finally, the term S_o is a constant background term due to thermal noise counts from the MPT. A computer code was written which adjusted the various terms, subject to the condition that the initial sublevel populations S_j have the ratios of statistical weights g_J = 2J + 1, or in the ratio S_1:S_2:S_3 = 2:4:6. The fitting procedure converged quickly because of the large lifetime differences in the sublevels.

One can express the goodness of fit between the fitting function $\mathscr{F}(t)$ and the data $d_i(t)$. The residuals Δ_i can be defined in terms of this difference, and the standard deviation σ_i of each data point, by $\Delta_i = [\mathscr{F}(t) - d_i(t)]/\sigma_i$. Here σ_i is calculated in Poisson statistics as the square root of the total number of counts (signal plus backgrounds) in each time bin. The measured distribution in Δ and results of the fit are given in Fig. 3. Other 2-4 term fits were tried, and as expected, showed a large degree of residual Δ difference between experiment and fit. One see that the residuals have converged about zero, and that there is good agreement between the data and fit, with no visible deviation from Gaussian statistics (rather than Poisson, since each channel had over hundred counts. Similar results were found in Ref. [7]. The probability distribution $P(\tilde{\chi}_d^2)$ for $\tilde{\chi}_d^2$ was calculated from the standard expression,

$$P(\tilde{\chi}_d^2) = \frac{1}{2^{d/2}\Gamma(d/2)} d(\tilde{\chi}_d^2 d)^{d/2-1} \exp(-\tilde{\chi}_d^2 d/2) \tag{5}$$

where d is the number of degrees of freedom in the present data, equal to 256 data bins minus 6 fitting parameters, or $d=250$. The data-fitting procedure was performed for each data set, and the resulting reduced $\bar{\chi}_d^2$ obtained. Results of all the five-exponential (six parameter) fits of the data are shown in Fig. 4 together with the Gaussian distribution $P(\bar{\chi}_d^2)$ as calculated in Eq.(5). The statistics are seen to be in good agreement with the $P(\bar{\chi}_d^2)$ distribution. The reduced $\bar{\chi}_d^2$ for all fits was centered at 1.00, with 56% of the data within the interval $\pm$ 0.0638, and 79% of the data within $\pm$ 0.1277. The reduced $\bar{\chi}_d^2$ region for 90% certainty is in the range $\pm$ 0.1476. It was experimentally observed that about 88% of the data fit within this region. The residuals Δ_i for each data run were also checked for the $\bar{\chi}_d^2$ distribution using a commercial statistical-graphics software package (Origen™). In this way other fits were tried, and those with only two exponential lifetime terms (a total of four exponentials and one constant background) gave a $\bar{\chi}_d^2$ larger than unity.

C. Effects of Collisional Quenching, and Results

Shown in Fig. 5 are the results for the Einstein A_J value from all runs. All data were taken with a pressure in the trap during operation of 1.3×10^{-7} Pa or less. A study of the effects of collisional quenching by the low pressures of background gas in the trap was made. It was found that under the low pressures of observation this effect was negligible. To see this, one notes that the measured decay rate $\mathbf{R}_m$ is given by the sum of the true decay rate A_J and the decay rate $\boldsymbol{R}_{trap}$ of ions in the trap:

$$\mathbb{R}_m = A_J + \mathbb{R}_{trap} \,. \tag{6}$$

The rate R_{trap} is in turn the sum of two modes of decay. One is the loss R_Q of metastable levels from all types of ion-gas collisional quenching (*i.e.*, recombination, charge-exchange, collisions of the second kind), and another R_{orbit} due to the orbital decay of the metastable through ion-surface collisions, or wayward ion trajectories. Using the Stern-Volmer concept, the collisional decay rate R_Q (s^{-1}) can be written as the product of a collisional rate constant k (cm^3/s) and the background gas density n_B (cm^{-3}). The rate R_{trap} is then,

$$\mathbb{R}_{trap} = \mathbb{R}_{orbit} + k_B n_B \,. \tag{7}$$

One may deliberately adjust the background gas density n_B and measure the total decay rate R_m at the various densities. A plot of R_m against n_B will then give the true Einstein rate A_J as the intercept, and the total effective rate constant k as the slope. This is true, since in practice the relation $R_{orbit} << A_J$ applied. This test was done by admitting N_2 gas into the trap, measuring the decay rates, then extrapolating the rates to zero n_B. The admitted gas density range was from the lowest operational density of 3×10^7 cm^{-3} (1.2×10^{-7} Pa) to 5×10^9 cm^{-3} (2×10^{-5} Pa). The extrapolated zero-pressure values obtained were the same as those in measurements made at the base operating pressure. Hence, the practice was established of using the trap lifetime as that measured by the channel electron multiplier (CEM in Fig. 2).

The final results of the lifetime measurements, with comparison to other measurements and calculations, are given in Table I. Agreement of the present data is consistent with the two other experimental results [7,8] given the combined error limits. No trends of data could be discerned. It is also seen that none of the four theoretical calculations gave the experimental results for *all three* sublevels. For example, the present summed rates from the $^4P_{1/2}$, $^4P_{3/2}$ and $^4P_{5/2}$ sublevels are 85%, 64%, and 93%, respectively, of the most-recently calculated values of Ref. [9]. The other experimental-theoretical comparisons clearly show that measurements are needed as inputs to astrophysical and fusion-plasma modeling codes. The experimental results can also serve as a benchmark for the theoretical calculations, so that the best theories can be used to compute, hopefully with unaltered accuracy, the myriad of transition probabilities for unresolved and/or higher-lying levels that are required for describing the hot solar, stellar, or fusion plasma.

ACKNOWLEDGMENTS

We thank E. Träbert for allowing us to cite his measurements prior to publication. We also acknowledge D. Moehs for discussions helpful in the setup and calibration of the trap, and D. Church for equipment loans and technical assistance. JBG thanks the National Research Council for fellowship support. This work was carried out at the Jet Propulsion Laboratory, California Institute of Technology, and was supported through the National Aeronautics and Space Administration.

References

[1] E. Vassiliadis, M. A. Dopita, R. C. Bohlin, J. P. Harrington, H. C. Ford, S. J. Meatheringham, P. R. Wood, T. P. Stecher and S. P. Maran, *Astrophys. J. Suppl. Ser. 114,* 237 (1998).

[2] A. A. Barth, G. A. Reichert, L. C. Ho, J. C. Shields, A. V. Fillipenko and E. M. Puchnarewicz, *Astron. J. 114,* 2313 (1997).

[3] H. R. Johnson, L. M. Ensman, D. R. Alexander, E. H. Avrett, A. Brown, K. G. Carpenter, K. Eriksson, B. Gustafsson, U. G. Jørgensen, P. D. Judge, J. L. Linsky, D. G. Luttermoser, F. Querci, M. Querci, R. D. Robinson and R. F. Wing, *Astrophy. J. 443,* 281 (1995).

[4] R. C. Isler, R. W. Wood, C. C. Klepper, N. H. Brooks, M. E. Fenstermacher and A. W. Leonard, *Phys. Plasmas 4,* 355 (1997).

[5] S. J. Smith, M. Zuo, A. Chutjian, S. S. Tayal and I. D. Williams, *Astrophys. J. 463,* 808 (1996).

[6] A. Chutjian, J. B. Greenwood and S. J. Smith, in *Atomic Processes in Plasmas* (eds. E. Oks and M. S. Pindzola, Am. Inst. Phys., NY 1998) p. 134.

[7] Z. Fang, V. H. S. Kwong, J. Wang and W. H. Parkinson, *Phys. Rev. A 48,* 1114 (1993).

[8] E. Träbert, G. Gwinner, X. Tordoir, E. J. Knystautas and A. Wolf, unpublished results. See also E. Träbert, A. Wolf, J. Linkemmann and X. Tordoir, *J. Phys. B. 32,* 537 (1999).

[9] D. J. Lennon, P. L. Dufton, A. Hibbert and A. E. Kingston, *Astrophys. J. 294,* 200 (1985).

[10] H. Nussbaumer and P. J. Storey, *Astron. Astrophys. 96,* 91 (1981).

[11] E. Dankworth and E. Treffitz, *Astron. Astrophys. 65,* 93 (1978).

[12] R. E. Stencel, J. L. Linsky, A. Brown, C. Jordan, K. G. Carpenter, R. F. Wing and S. Czyzak, *Mon. Not. Roy. Astron. Soc. 196*, 47 (1981).

[13] S. Bashkin and J. O. Stoner, Jr., *Atomic Energy Levels and Grotrian Diagrams 1* (American Elsevier, NY, 1975).

[14] J. B. Greenwood, S. J. Smith, A. Chutjian and E. Pollack, *Phys. Rev. A 59*, 1348 (1999), and references therein.

[15] J. B. Greenwood, A. Chutjian and S. J. Smith, *Astrophys. J.*, in press.

[16] D. A. Church, *Physics Reports 228*, 253 (1993).

[17] R. R. Lewis, *J. Appl. Phys. 53*, 3975 (1982); *Phys. Rev. A 28*, 1228 (1963).

[18] L. Yang, D. A. Church, S. Tu and J. Jin, *Phys. Rev. A 50*, 166 (1994).

[19] L. Yang and D. A. Church, *Nucl. Instr. Methods B56/57*, 1185 (1991).

Table I. **Summary of Measured and Calculated Transition Probabilities for the $2s^22p\ ^2P^o - 2s2p^2\ ^4P$ Transitions in C^+.**

Transition	Measured A_J (s^{-1})			Calculated A_J (s^{-1})			
	Present	Ref. [7]	Ref. [8]	Ref. [9]	Ref. [10,12]	Ref.[10]	Ref. [11]
$^4P_{1/2} \rightarrow {}^2P_{1/2}$				74.4	56.4	55.3	42.5
$^4P_{1/2} \rightarrow {}^2P_{3/2}$				77.8	65.7	65.5	40.2
$^4P_{1/2} \rightarrow {}^2P_{1/2,3/2}$	130.0 ± 5.5	146.4 (+8.3,-9.2)	125.8 ± 0.9	152.2	122.1	120.8	82.7
$^4P_{3/2} \rightarrow {}^2P_{1/2}$				1.70	2.8	1.71	1.01
$^4P_{3/2} \rightarrow {}^2P_{3/2}$				12.4	8.5	5.24	8.11
$^4P_{3/2} \rightarrow {}^2P_{1/2,3/2}$	9.0 ± 1.0	11.6 (+0.8,-1.7)	9.63 ± 0.02	14.1	11.3	6.95	9.12
$^4P_{5/2} \rightarrow {}^2P_{3/2}$	50.0 ± 2.5	51.2 (+2.6,-3.5)	45.37 ± 0.17	53.9	37.6	43.2	34.4

Figure Captions

Figure 1. Energy level diagram for the $2s^2 2p\ ^2P^o$- $2s2p^2\ ^4P$ transitions of C^+. Energies of the sublevels are given in cm^{-1} above the ground state, and emission wavelengths are in Å.

Figure 2. Schematic diagram of the Kingdon ion trap for measuring lifetimes in highly-charged ions. The components are: **ECR** mass/charge selected beam from the ion source, **SW** three-way electrostatic beam switcher, **L1** - **L2** ion lenses, **L3** - **L4** photon lenses, **IS** ion shield grid, **IF** interference filter, **MPT** multiplier phototube, **FC** incident ion beam Faraday cup, **MCP** microchannel plate for detection of ions in the trap, **MCS** signals to PC-controlled multichannel scalers, **KT** Kingdon trap cylinder, **CB** cylinder bias, and **W** central wire. The incident **ECR** beam may also be directed at **SW** to separate charge exchange (**CE**) and excitation (**EX**) experimental areas.

Figure 3. Decay curves for the $2s2p^2\ ^4P \rightarrow 2s^2 2p\ ^2P^o$ optical emissions at 232 nm. Inset **a** shows the decay in the range 0-50 msec, and **b** the decay over the entire measured time duration 0-200 msec.

Figure 4. Residuals of the fitting procedure, showing the number of hits of a residual value Δ versus that value of Δ. To demonstrate the degree of fit, the solid line is the

Gaussian distribution $P(\Delta) = (2\pi)^{-1/2} \exp(-\Delta^2/2)$.

Figure 5. Values of $\bar{\chi}_d^2$ with the five-exponential (six parameter) fit of the data. Horizontal dashed lines are the limits within which 90% of all data should lie. The calculated Gaussian distribution $P(\bar{\chi}_d^2)$ is shown at the right.

Figure 6. The Einstein $A_{1/2}$, $A_{3/2}$ and $A_{5/2}$ values (top to bottom) for emission from the $2s2p^2\ {}^4P$ state, as recorded for individual runs. Horizontal lines correspond to the average values of 130.0 s^{-1}, 8.90 s^{-1}, and 50.0 s^{-1} for J = 1/2, 3/2, and 5/2, respectively.

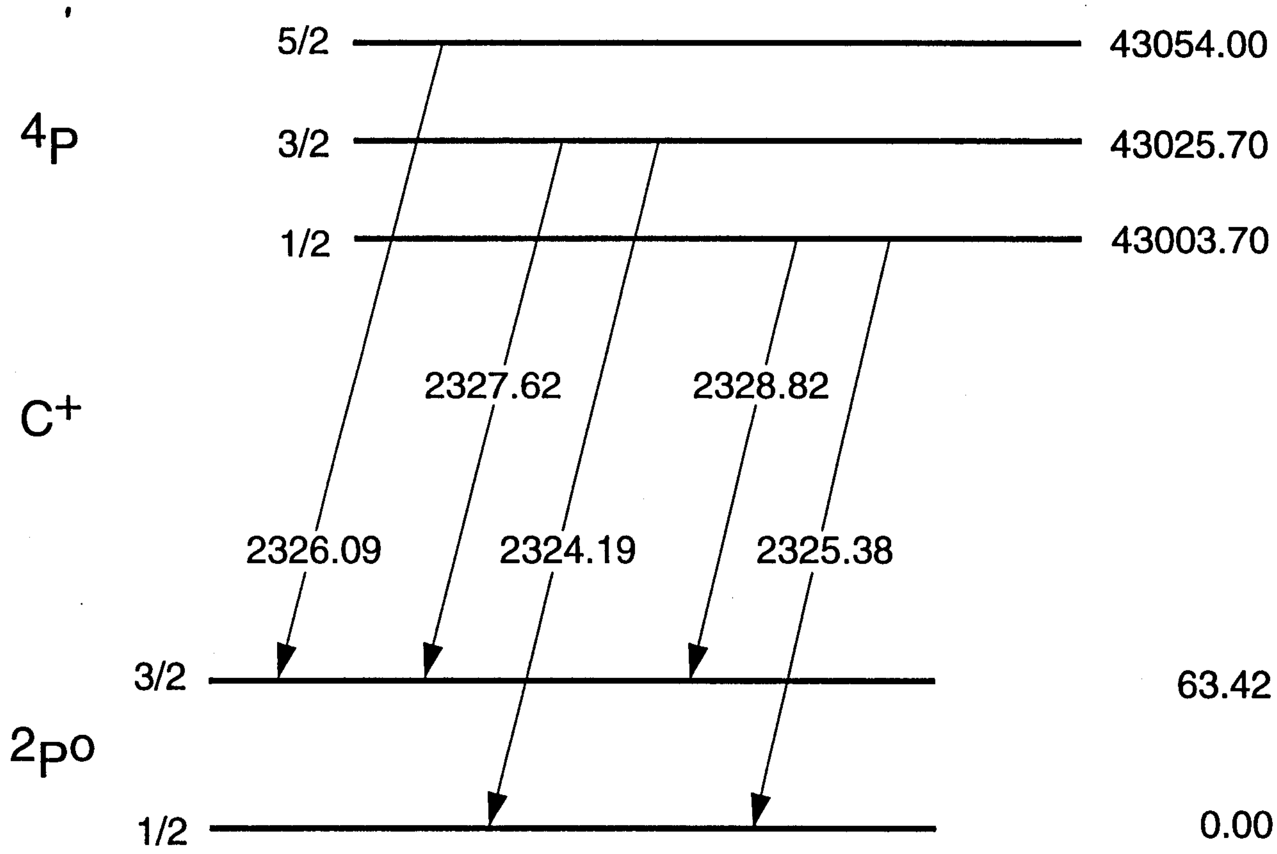
4P
C+
2Po
5/2
3/2
1/2
3/2
1/2
43054.00
43025.70
43003.70
63.42
0.00
2327.62
2328.82
2326.09
2324.19
2325.38

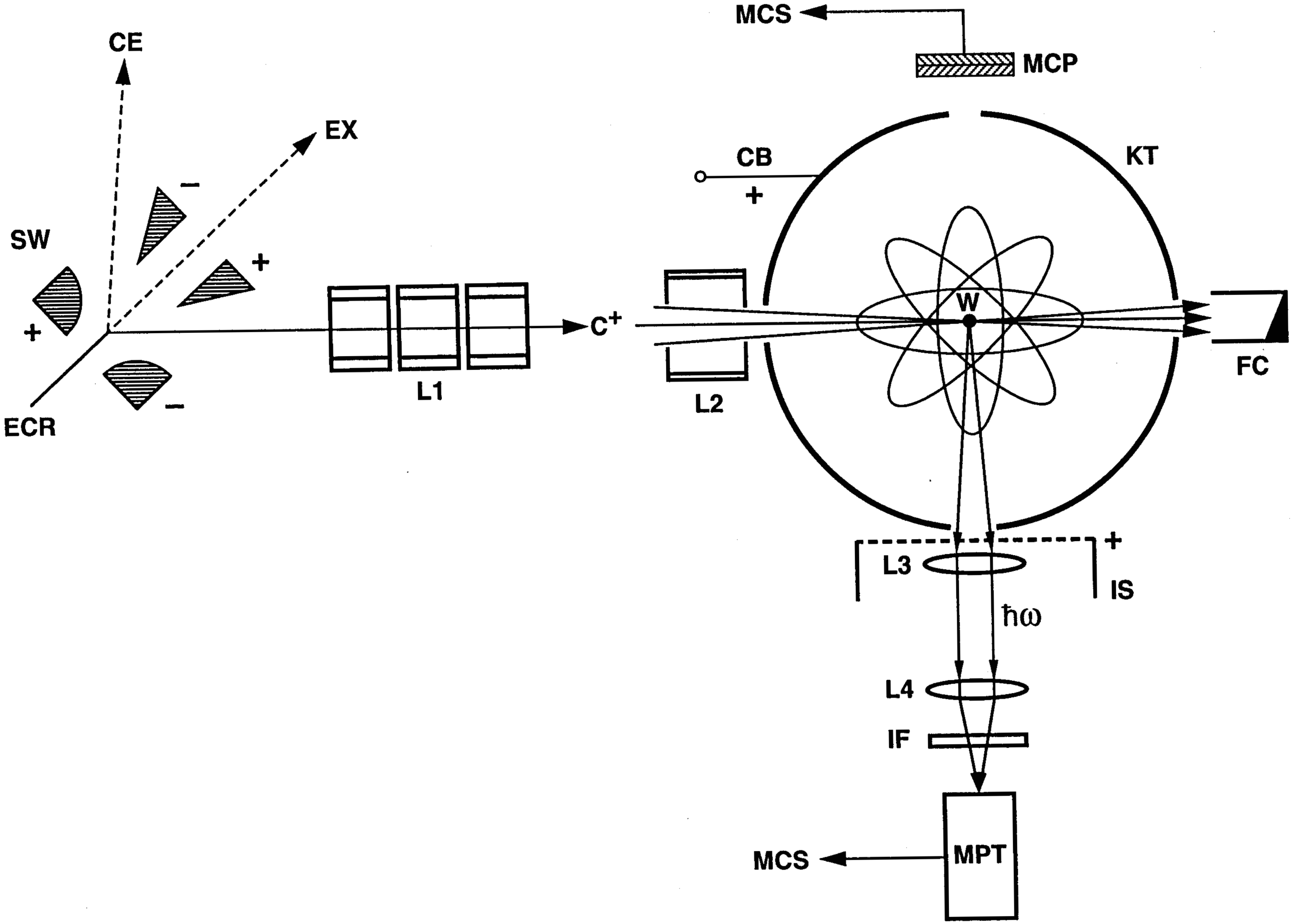

2

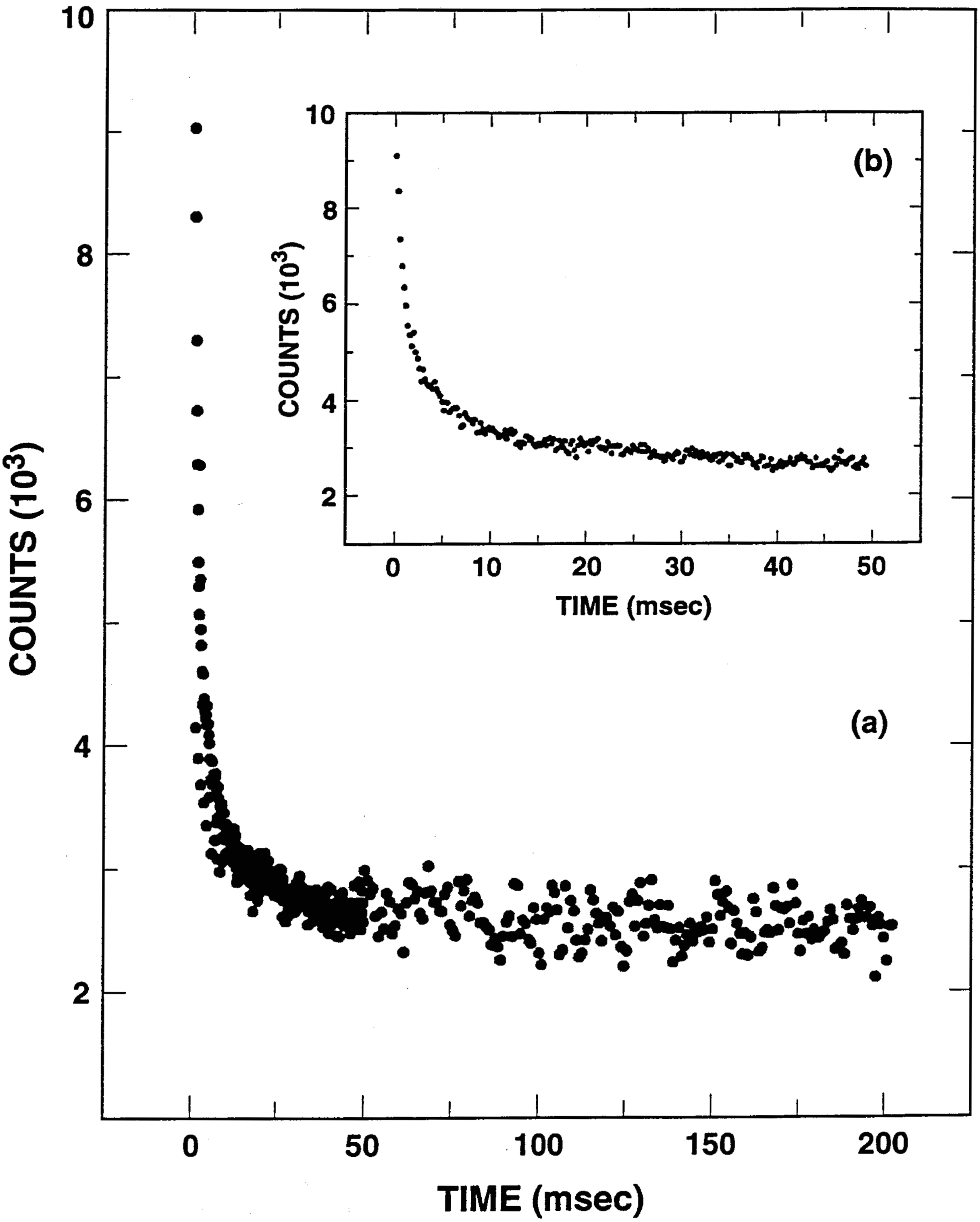

COUNTS (10^3)
TIME (msec)
(a)
(b)
10
8
6
4
2
0
10
20
30
40
50
100
150
200

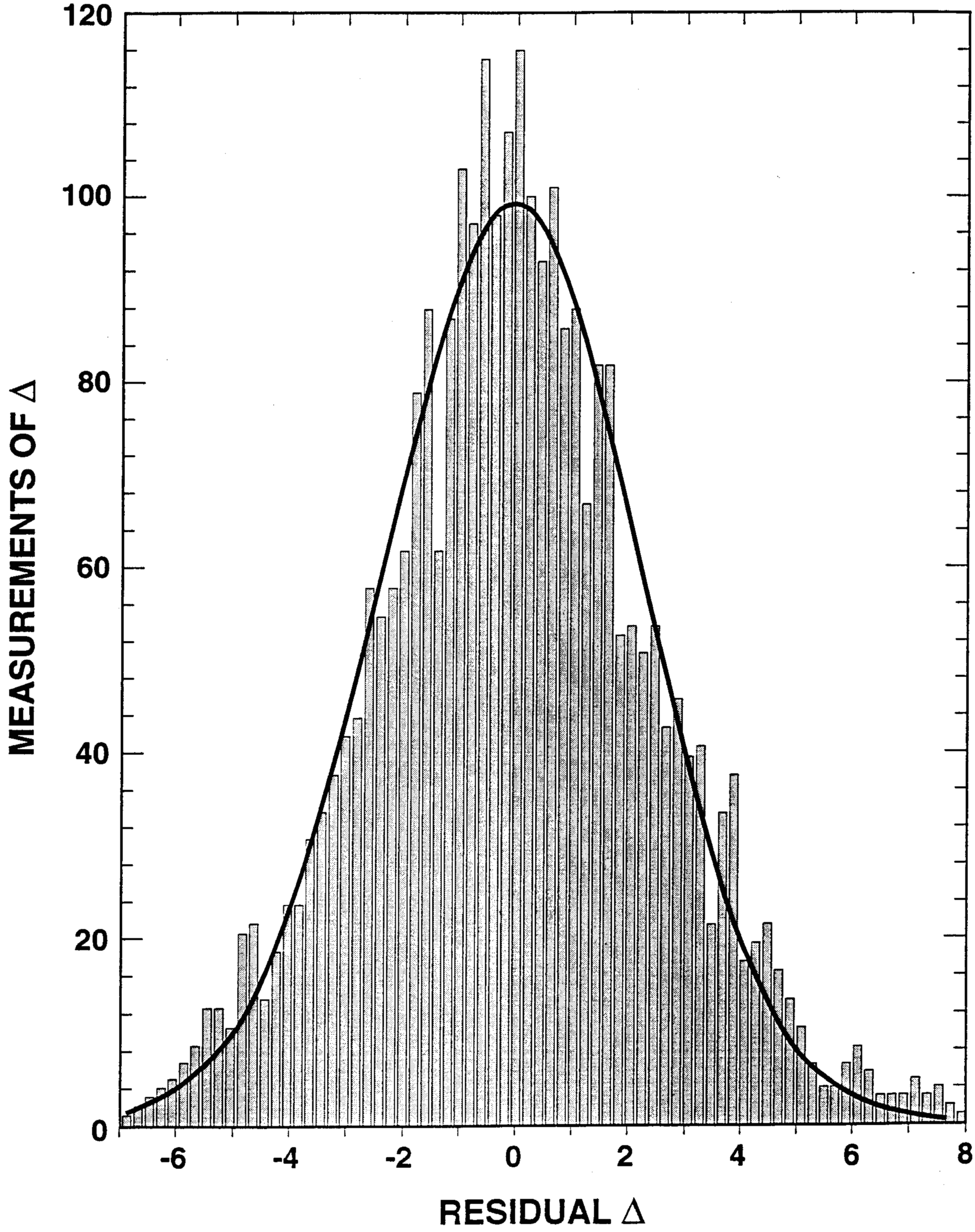
120
100
80
60
40
20
0
MEASUREMENTS OF Δ
-6
-4
-2
0
2
4
6
8
RESIDUAL Δ

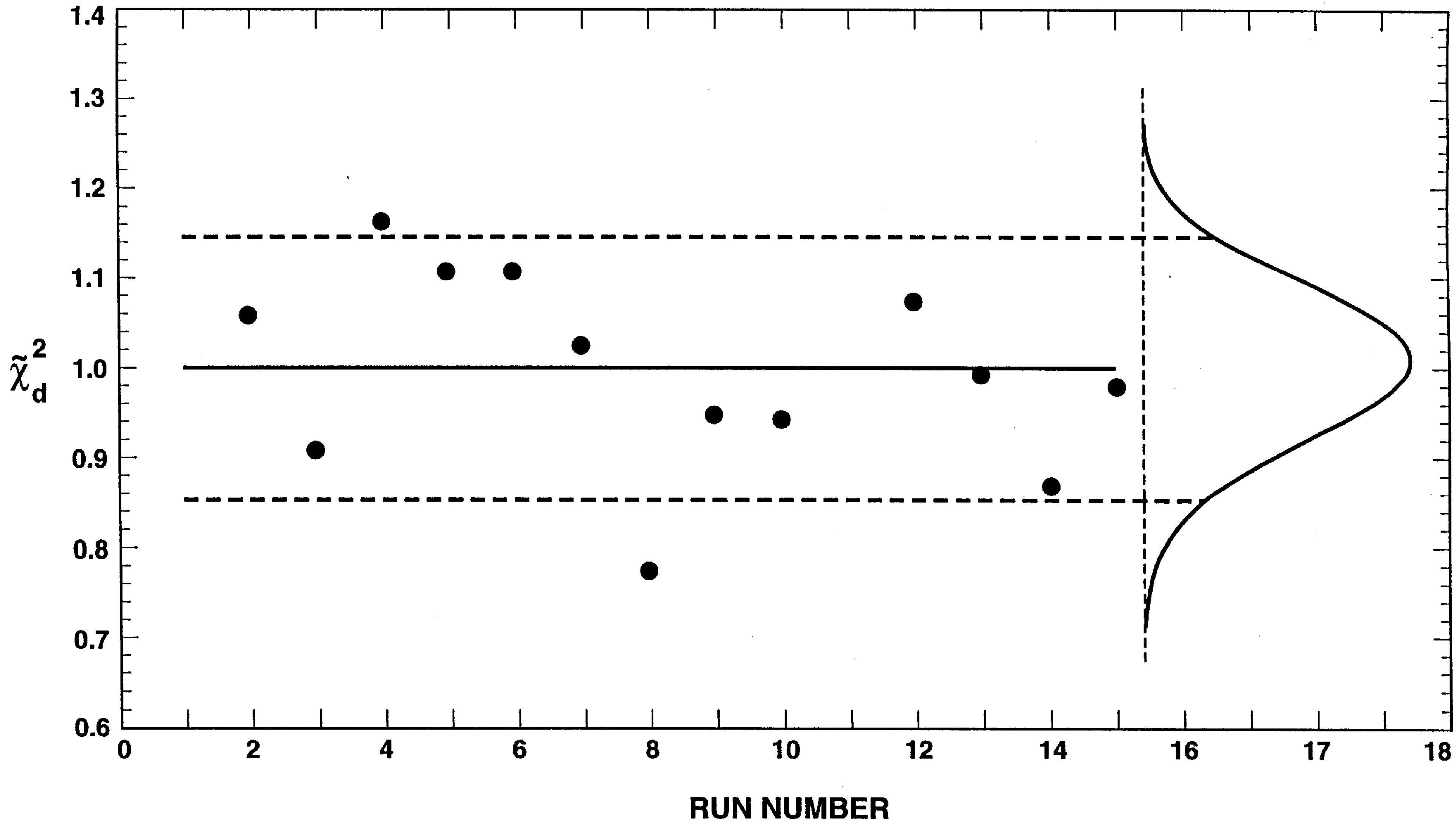

1.4
1.3
1.2
1.1
1.0
0.9
0.8
0.7
0.6
$\tilde{\chi}_d^2$
0
2
4
6
8
10
12
14
16
17
18
RUN NUMBER

5

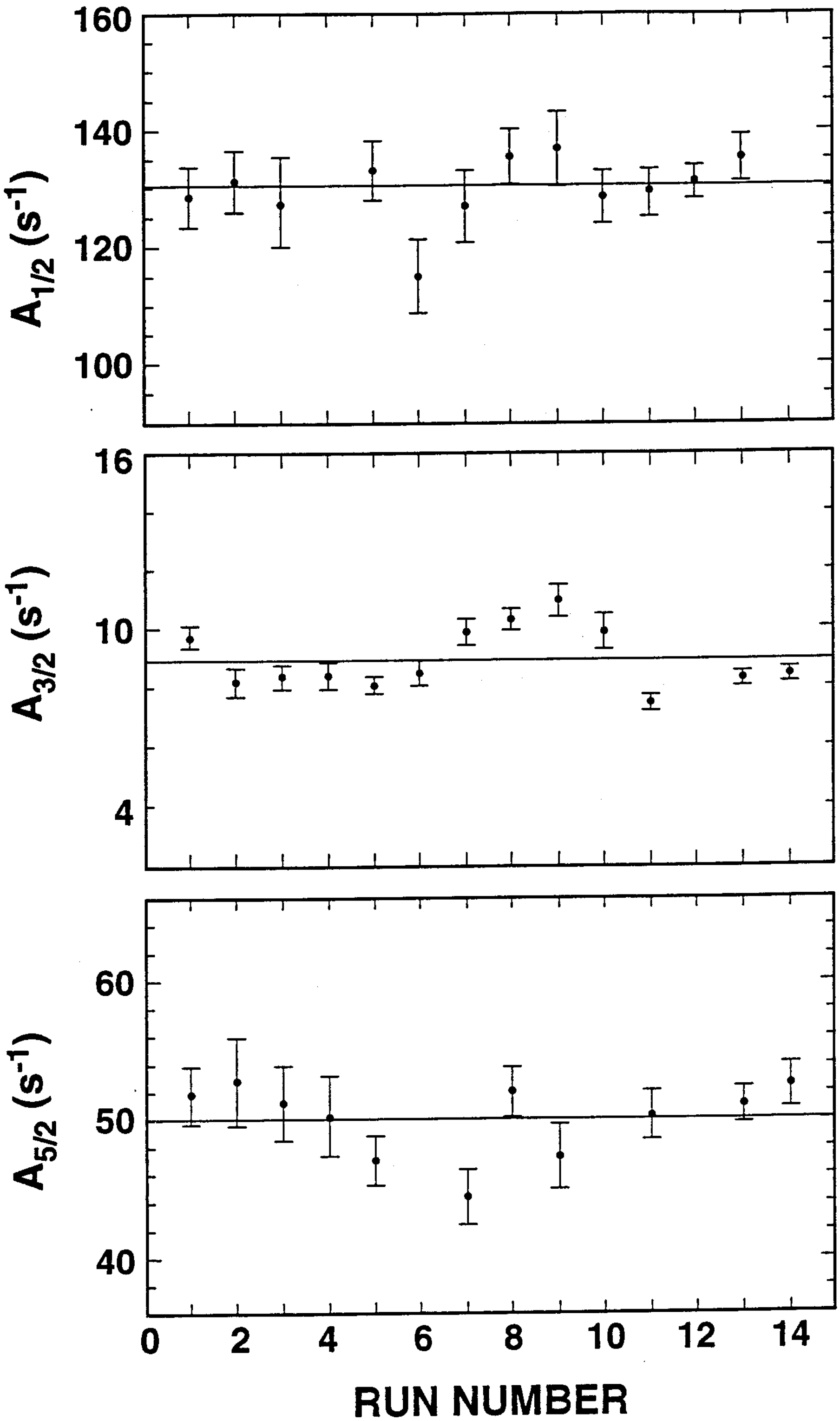

160
140
120
100
$A_{1/2}$ (s^{-1})
16
10
4
$A_{3/2}$ (s^{-1})
60
50
40
$A_{5/2}$ (s^{-1})
0
2
4
6
8
10
12
14
RUN NUMBER